Appendix 3

Titus Kuehne, MD
Maythem Saeed, DVM, PhD
Charles B. Higgins, MD
Kelly Gleason, MD
Gabriele A. Krombach, MD
Oliver M. Weber, PhD
Alastair J. Martin, PhD
Daniel Turner, MD
David Teitel, MD
Phillip Moore, MD

Index terms:
Animals
Heart, interventional procedures, 533.1269, 564.1269
Heart, MR, 56.121419
Heart, valves, 533.1269
Pulmonary arteries, 564.1269
Stents and prostheses, 533.1269, 564.1269

Published online before print
10.1148/radiol.2262011639
Radiology 2003; 226:475–481

[1] From the Department of Radiology (T.K., M.S., C.B.H., G.A.K., O.M.W.) and the Division of Pediatric Cardiology (T.K., K.G., D. Turner, D. Teitel, P.M.), University of California San Francisco, 505 Parnassus Ave, L308, San Francisco, CA 94143-0628; Institute for Biomedical Engineering, Swiss Federal Institute of Technology and University of Zurich, Switzerland (O.M.W.); and Philips Medical Systems, Best, the Netherlands (A.J.M.). Received October 5, 2001; revision requested December 18; final revision received May 31, 2002; accepted July 10. **Address correspondence to** C.B.H. (e-mail: *charles.higgins@radiology.ucsf.edu*).

Author contributions:
Guarantors of integrity of entire study, T.K., M.S., C.B.H., P.M.; study concepts and design, T.K., P.M., M.S., O.M.W., C.B.H.; literature research, T.K., M.S.; experimental studies, T.K., M.S., P.M., K.G., D. Turner, G.A.K., D. Teitel, O.M.W.; data acquisition, T.K., M.S., O.M.W., K.G., A.J.M.; data analysis/interpretation, T.K., M.S., P.M., G.K., K.G., D. Turner, G.A.K., D. Teitel, O.M.W.; statistical analysis, T.K., M.S.; manuscript preparation, T.K., M.S.; manuscript definition of intellectual content, T.K., M.S., C.B.H.; manuscript editing, revision/review, and final version approval, all authors.

Endovascular Stents in Pulmonary Valve and Artery in Swine: Feasibility Study of MR Imaging–guided Deployment and Postinterventional Assessment[1]

PURPOSE: To assess the feasibility of using magnetic resonance (MR) imaging to guide stent deployment in the pulmonary valve and artery and evaluate, after stent deployment, the position and morphology of and blood flow through the stent.

MATERIALS AND METHODS: Angiography and 1.5-T MR imaging were performed in a dual-imaging suite. Nitinol stents were placed in the pulmonary valve and main pulmonary artery in five pigs by using MR imaging guidance. For interactive MR imaging monitoring of catheter manipulation and stent delivery, balanced fast field-echo and T1-weighted turbo field-echo sequences were used. Visualization of the delivery system was based on T2* (with air as the contrast material) or T1 (with gadodiamide as the contrast material). After stent deployment, the position and morphology of and flow through the stent were verified with multiphase multisection balanced fast field-echo and velocity-encoded cine MR imaging. Findings at angiography and postmortem examination also helped verify stent placement. The paired Student *t* test was used for data analysis.

RESULTS: The stent was successfully deployed in all animals. The stent was placed distal to the pulmonary valve in four animals and across the pulmonary valve in one animal. The position and morphology of the stent were clearly depicted on balanced fast field-echo images. In the animal with the stent placed across the pulmonary valve, the pulmonary regurgitant fraction was 37%; this was not seen in the animals with stents placed distal to the pulmonary valve. No complication (eg, stent migration, intramural injury, or vascular perforation) was noted during the intervention. Findings at angiography and postmortem examination confirmed the position of the stents.

CONCLUSION: MR imaging has the potential to guide stent placement in the pulmonary valve or artery and to evaluate flow volume within the stent lumen after the intervention.

Many congenital heart defects are associated with pulmonary insufficiency or stenosis. After surgical repair of the tetralogy of Fallot, these lesions may remain to variable degrees. The resultant isolated or combined pressure-volume overload of the right ventricle can lead to severe and irreversible heart failure (1,2).

Endovascular and valved stents have been successfully placed for the treatment of pulmonary obstruction and insufficiency (3,4). However, patients are often left with residual pulmonary insufficiency and the risk of restenosis (5–7). Close monitoring of such patients is essential to prevent heart failure. To minimize radiation exposure imposed by repetitive cardiac catheterization in children, a nonradiographic imaging technique is desirable to monitor (*a*) cardiac and pulmonary anatomy, (*b*) ventricular function,

(*c*) quantitative blood flow volumes in the aorta and native and stented pulmonary arteries, and (*d*) interventional procedures.

Findings in several studies have validated the accuracy of magnetic resonance (MR) imaging for assessing the anatomy and function of the heart and great arteries (8–11). The recent implementation of fast MR imaging sequences along with the ability of MR imaging to acquire images in any given orientation and with high soft-tissue contrast makes this technique attractive for guiding interventional procedures. Indeed, MR imaging–guided endovascular interventions have been performed in the aorta, iliac and femoral arteries, and vena cava (12–15). MR imaging–guided cardiopulmonary interventions, however, are more challenging due to motion artifacts caused by the beating heart and respiration. Moreover, the tortuous anatomy of the right cardiac chambers and pulmonary arteries makes monitoring of the passage of guide wires and endovascular catheters and the deployment of stents with MR imaging more difficult.

The purpose of the present study was to guide stent deployment in the pulmonary valve and artery and to evaluate, after stent deployment, the position and morphology of and pulmonary blood flow through the stent.

MATERIALS AND METHODS

Study Protocol

All procedures were performed in accordance with National Institutes of Health guidelines for the care and use of laboratory animals and with the approval of the Infection Control Committee and the Committee of Animal Research at the University of California, San Francisco. With MR imaging guidance, endovascular nitinol stents were placed across or distal to the pulmonary valve in five pigs (weight, 20–27 kg). After stent placement, pulmonary blood flow volumes within the stent lumen were assessed with velocity-encoded cine MR imaging.

Experiments were performed in a laboratory consisting of an angiographic unit (Integris V5000; Philips Medical Systems, Best, the Netherlands) and a 1.5-T short-bore MR unit (Intera I/T; Philips Medical Systems, Best, the Netherlands) (Fig 1). The units, which were integrated into two adjoining rooms, were connected with a sliding table. This arrangement enabled us to perform interventional procedures with combined angiographic and MR imaging guidance without changing the position of the animal. A sliding door that was impenetrable to x-ray and radiofrequency power separated the two rooms.

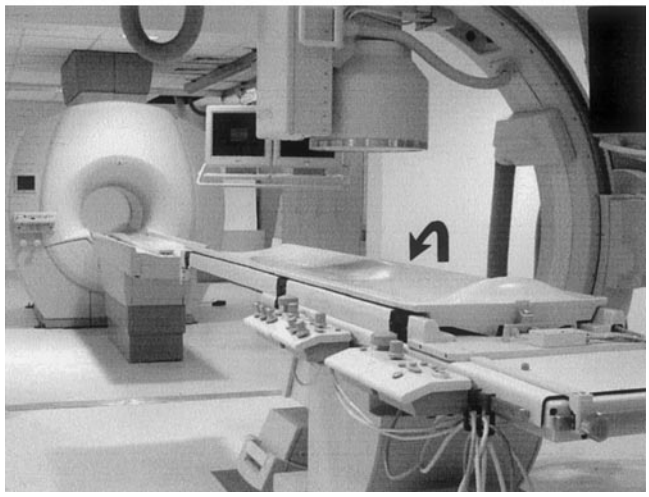

Figure 1. Interventional MR imaging and angiography suite used in the present study. The two adjoining units are connected by a sliding table (arrow), which allows transport of a subject from one unit to the other without changing position.

Animals were anesthetized with intramuscular injection of a mixture of 0.025 mg per kilogram of body weight of telazol (Wildlife Pharmaceuticals, Fort Collins, Colo), ketamine (Ketaset; Fort Dodge Laboratories, Fort Dodge, Iowa), and xylazine (Anased Injection; Lloyd Laboratories, Shenandoah, Iowa). This was followed by 2% isofluorane inhalation (IsoFlo; Abbott Laboratories, North Chicago, Ill) for maintenance of general anesthesia. After completion of the experiment, animals were euthanized with sodium pentobarbital (200 mg/kg intravenously) (Abbott Laboratories). The heart rate, systemic blood pressure, and arterial blood oxygen saturation were continuously monitored during the experiment.

Characteristics of the Stents and Delivery System

The self-expanding nitinol stent (Memotherm; Angiomed, Karlsruhe, Germany) consisted of a laser-cut metal alloy composed of 50% titanium and 50% nickel. The stent material is nonmagnetic and yields a susceptibility value of -7×10^{-6} to -11×10^{-6}. Fully expanded stents were 18 mm in diameter and 25 mm long.

The stent delivery system was composed of a 9-F-long sheath, 9-F dilator, and 6-F balloon catheter. The stents were mounted on the tip of the long sheath. The dilator and catheter were integrated inside the lumen of the long sheath with the balloon tip of the catheter positioned through the stent at the distal end. The balloon was inflated with either air or 1% solution of gadodiamide (0.5 mol/L stock solution) (Omniscan; Amersham Health, Buckinghamshire, England). The stent delivery system, which was guided into a pulmonary position over a 0.035-inch guide wire (Microvena, White Bear Lake, Minn), was composed of a nitinol shaft and a 9-mm-long floppy stainless steel tip. When the stent was in the desired position, it was deployed by advancing the dilator, which pushed the stent out of the long sheath.

MR Imaging

MR imaging was performed by using an array of two phased circular receiver coils (coil diameter, 20 cm). The intervention was guided from an in-room operating console and displayed on a monitor adjacent to the magnet. All imaging was guided interactively. Real-time image acquisition of the anatomic structures and passive position monitoring of the interventional instruments were partially performed with cardiac gating (gating delay, 320 msec) by using four-lead vector electrocardiography. For image acquisition, balanced fast field-echo and T1-weighted turbo field-echo sequences were used. The quality of the images obtained with the two pulse sequences were compared in consensus (T.K., M.S., O.M.W., A.J.M.). Balanced fast field-echo is a steady-state free precession sequence. Image contrast between the interventional instruments and the surrounding

anatomy was achieved in two ways. Susceptibility-based contrast was used to monitor the position of the guide wire, mounted stent, dilator, and balloon of the catheter when filled with air. The balloon was visualized alternatively as a bright spot on the T1-weighted turbo field-echo images when filled with gadodiamide. Contrast between the heart or great vessels and interventional instruments was determined subjectively (T.K., M.S., O.M.W., D.Turner, P.M.).

Acquisition parameters for the balanced fast field-echo sequence were as follows: 3.4/1.7 (repetition time msec/echo time msec), 128 × 128 matrix, 300 × 300-mm field of view, 5–30-mm-thick sections, 60° flip angle, and single-shot acquisition of 454 msec. Acquisition parameters for the T1-weighted turbo field-echo sequence were as follows: 3.9/1.3, 240 × 168 matrix (image percentage of 70%), 240 × 300-mm field of view (80% rectangular field of view), 5–30-mm-thick sections, 60° flip angle, and acquisition time of 510 msec. T1 enhancement was achieved with radio-frequency spoiling. After stent deployment, the stent position was verified by means of an electrocardiography-gated multicardiac phase balanced fast field-echo sequence. Imaging parameters were as follows: 3.0/1.5, 176 × 211 matrix (image percentage of 120%), 255 × 320-mm field of view (80% rectangular field of view), 8-mm-thick sections, and 50° flip angle. Sixteen to 50 phase images were acquired during free breathing. A velocity-encoding cine sequence was used to quantify pulmonary blood flow volumes within the stent lumen. All velocity-encoding cine MR measurements were made in a double oblique plane perpendicular to the dominant flow direction in the main pulmonary artery (T.K., M.S.). This plane was positioned in the middle of the stent. The sequence was gated retrospectively, and 16 cardiac phase images were acquired. The following acquisition parameters were used: 15/3.8, 128 × 128 matrix, 150 × 150-mm field of view, 5-mm-thick sections, 15° flip angle, two signals acquired, and velocity encoding of 200 cm/sec/π.

Interventional Procedure

An 11-F sheath (Cook, Indianapolis, Indiana) was placed into the femoral vein with angiographic guidance. The length of the coil used for MR guidance of the balloon catheter was approximately from the level of the kidneys to above the aortic arch. The animal and bed were examined visually and scanned with a portable metal detector before the table was moved from the angiographic unit into the bore of the MR imager (Fig 1). The time required to transfer the animal from the angiographic room into the MR imager was less than 3 minutes, and the first image was obtained 5–10 minutes after the start of the transfer.

Guide wire position.—In the MR unit, a 6-F balloon tip catheter was inserted into the inferior vena cava and the balloon filled with gadodiamide. Insertion of interventional devices was facilitated by using an extended introducer sheath so as to enable device handling from outside the magnet bore without changing the position of the animal. The catheter and guide wire were introduced via the femoral vein and moved forward to the inferior vena cava, right atrium, right ventricle, and into the pulmonary position during imaging. This catheter was then advanced through the right side of the heart into the main pulmonary artery. Cardiac-gated T1-weighted turbo field-echo imaging was performed in the parasagittal plane to monitor catheter advancement and position (O.M.W., M.S., T.K., K.G., P.M.).

Advancement of the balloon tip catheter from the main pulmonary artery into the distal pulmonary bed was monitored in the paracoronal plane. Arterial and venous blood pressures were continuously recorded to determine the effect of the intervention on blood pressure and to confirm the course of the balloon tip catheter through the inferior vena cava, right ventricle, main pulmonary artery, and distal pulmonary bed. Once the balloon of the catheter was positioned in a distal pulmonary arterial branch at the margin of the lung and just adjacent to the diaphragm, the guide wire was advanced through the lumen of the catheter. The intended wire position, with the tip in a distal pulmonary artery, was confirmed when susceptibility artifacts were noted in the periphery of the lung just above the diaphragm.

Stent deployment.—The stent delivery system was advanced over the guide wire into the pulmonary position. The balloon at the tip of the delivery system was filled with either air or gadodiamide to enable visualization of the catheter tip with MR imaging. Manipulation of the catheter from the inferior vena cava into the pulmonary artery was monitored with T1-weighted turbo field-echo imaging in the parasagittal plane after the balloon was filled with gadodiamide. Advancement of the delivery system through the right ventricular chamber often caused ventricular ectopia. Therefore, cardiac gating was not used during this phase. Once the tip of the delivery system was seen in the main pulmonary artery, monitoring was performed with a balanced fast field-echo sequence in the paratransverse plane by using the air-filled balloon at the tip of the delivery system. It took 3–5 minutes to advance the delivery system through the right ventricular chamber. The distance between the pulmonary valve and the bifurcation of the left and right pulmonary arteries was measured (T.K., K.G., D.Turner, P.M.). The stents were deployed when the distal tip of the delivery system was about 10 mm distal to the pulmonary valve (T.K., K.G., P.M.). The intended locations of the deployed stents were in the pulmonary valve and main pulmonary artery.

Functional and morphologic assessment of the stent.—After stent placement, right ventricular and pulmonary artery blood pressures were measured by using a 7-F wedge catheter. Flow volume measurements within the stent lumen were performed with velocity-encoding cine MR imaging (16,17). The position and morphology of the stent and pulmonary artery were verified with paratransverse and parasagittal balanced fast field-echo images (O.M.W., M.S., T.K.). The signal-to-noise ratio was measured on balanced fast field-echo images within the lumen of the stent and compared with that in the center of the main pulmonary artery distal to the stent. The extent of susceptibility artifacts at the stent wall was measured as the number of pixels that yielded signal void. The extent of susceptibility artifacts was measured on balanced fast field-echo images and compared with measurements acquired on T1-weighted turbo field-echo images.

After the interventional procedure and MR imaging, the animals were brought back into the angiographic unit to reevaluate the stent position and determine whether any complication or arterial injuries had occurred during the MR imaging–guided procedure (T.K., K.G., P.M.). Angiograms were obtained during injection of a bolus of an iodinated contrast material (Omnipaque, 8 mL; Amersham Health) by using a 7-F Berman or wedge catheter (Arrow, Reading, Pa). Blood pressure was measured in the right ventricle and main pulmonary artery by using a 7-F wedge catheter. Pressure measurements were compared with those obtained during MR imaging after stent placement. After euthanasia, the hearts and its great vessels

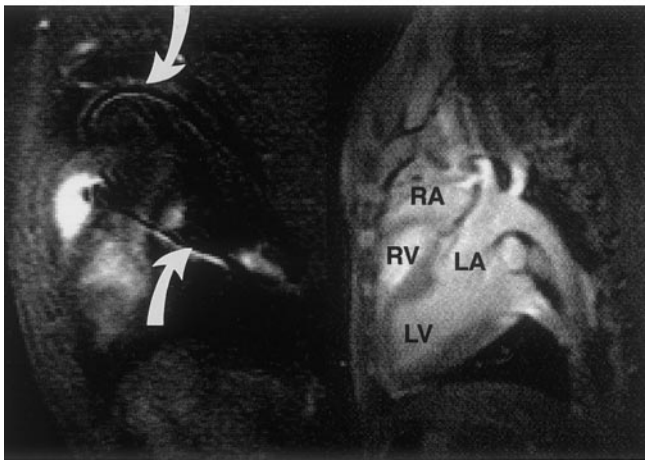

Figure 2. (Left) Oblique sagittal T1-weighted turbo field-echo MR image (3.9/1.3) and (right) balanced fast field-echo MR image (3.4/1.7) of the heart and great vessels. Note good contrast between guide wire and background anatomy on T1-weighted turbo field-echo image (arrows). Curvature information for the guide wire was obtained along the tortuous anatomy of the inferior vena cava, right atrium *(RA)*, right ventricular outflow tract, and pulmonary artery by using a section thickness of 30 mm. Conversely, the corresponding electrocardiography-gated balanced fast field-echo image (section thickness, 5 mm) contains detailed anatomic information. *RV* = right ventricle, *LA* = left atrium, *LV* = left ventricle.

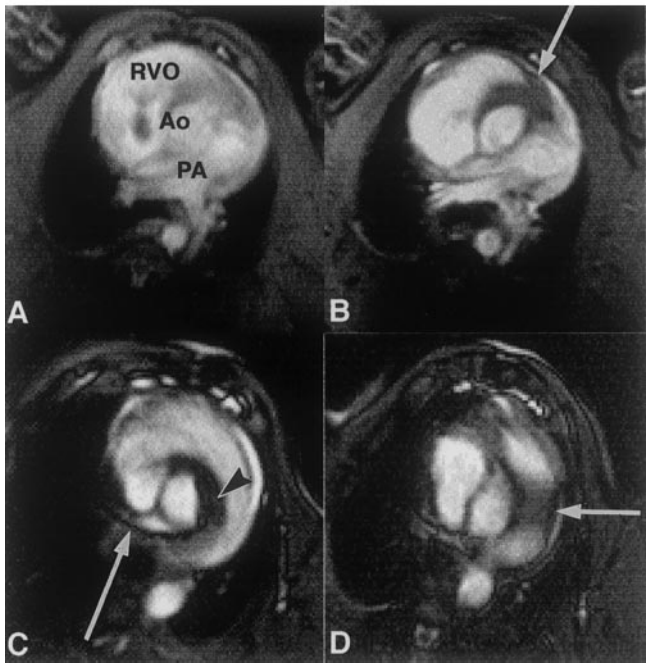

Figure 3. Series of oblique transverse balanced fast field-echo MR images (3.4/1.7, 7-mm-thick sections). *A,* Image obtained through right ventricular outflow tract *(RVO)* and pulmonary artery *(PA)*. *Ao* = aorta. *B,* Image shows guide wire and stent delivery system across pulmonary valve (arrow). *C,* Stent was released when tip of application system (arrowhead) was seen approximately 10 mm distal to the pulmonary valve (arrow). *D,* Image shows stent (arrow) immediately after deployment.

were excised and examined for the position and morphology of the stent and morphology of the pulmonary valve and pulmonary artery.

Statistical Analysis

Data are presented as means ± SDs. The paired Student *t* test was applied because in the same group of animals we compared (*a*) signal-to-noise ratios measured with balanced fast field-echo imaging within the lumen of the stent and distal to the stent, (*b*) the extent of susceptibility measured with balanced fast field-echo versus T1-weighted turbo field-echo imaging, and (*c*) the peak systolic pressure within the right ventricle and pulmonary artery during MR imaging and those during angiography. Differences with a *P* value of less than .05 were considered statistically significant.

RESULTS

Interventional Procedure

Stent deployment in the pulmonary valve and main pulmonary artery was successful in all five animals. The stent was placed across the pulmonary valve in one animal and in the main pulmonary artery in four animals. In the four animals, the stent was 1–3 mm distal to the pulmonary valve in three and 7 mm distal to the pulmonary valve in one.

The quality of the images of the heart and great arteries was better with the balanced fast field-echo sequence than with the T1-weighted turbo field-echo sequence (Fig 2). Balanced fast field-echo images showed the main pulmonary artery with the pulmonary valve leaflets and the left and right pulmonary arteries. They also provided relatively better contrast between the blood pool (high signal intensity) and interventional instruments (signal void) (Fig 3). Unequivocal definition of the tip of the catheters, however, was not always achievable.

With the T1-weighted turbo field-echo sequence, it was necessary to use thick sections (20–30 mm) to monitor catheter movement inside the cardiac chambers and throughout the tortuous right ventricular outflow tract. Use of thick sections with balanced fast field-echo imaging, however, caused substantial partial volume effects and limited visualization of interventional instruments, which were depicted as signal voids (Fig 2). Catheters and guide wires tended less to out-of-plane motion when imaging was performed at the level of the main pulmonary artery. At this site, thin sections (5–10 mm) were required to visualize the interventional instruments and surrounding tissue on balanced fast field-echo images.

Visualization of the gadodiamide–doped balloon was not affected by partial volume effects, even with a section thickness of 30 mm on T1-weighted turbo field-echo images. Therefore, MR imaging guidance of catheters within the cardiac chamber and right ventricular outflow tract was performed by using the T1-weighted turbo field-echo sequence. The high signal intensity derived from the gadodiamide-filled balloon was also distinguishable from the low-signal-intensity background of the lung (Fig 4). This was crucial for accurate localization of the tip of the catheter in the pulmonary bed and, consecutively, adequate positioning of the guide wire.

The floppy stainless steel tip of the guide wire caused only minor artifacts when contained inside the guiding balloon catheter. The artifact size, however, increased substantially when the tip of the guide wire was brought outside the catheter. The appearance of artifacts was rapidly and unambiguously localized on

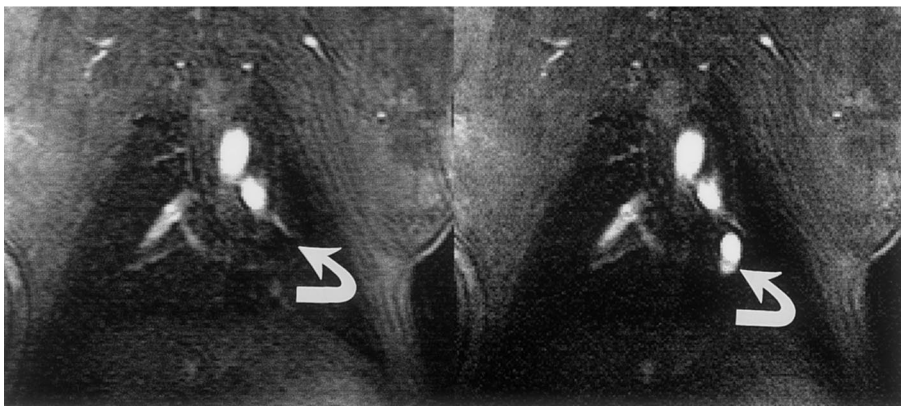

Figure 4. Oblique coronal T1-weighted turbo field-echo MR images (3.9/1.3) of lung. Tip of balloon catheter was filled with either (left) air (arrow) or (right) 1% solution of gadodiamide (arrow). Visualization of air-filled balloon against low-signal-intensity background of lung was not possible. In contrast, gadodiamide–doped balloon was reliably visualized and helped confirm position of catheter tip in distal branch of pulmonary arteries.

Figure 5. Multisection multiphase balanced fast field-echo image (3.4/1.7) shows postinterventional assessment of pulmonary artery and stent positioned across pulmonary valve. Depiction of wall of pulmonary artery adjacent to stent is partially superimposed by susceptibility artifacts of stent (signal void, arrow).

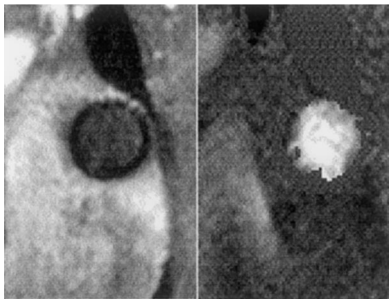

Figure 6. Velocity-encoding cine MR images (15/3.8) of pulmonary artery. (Left) magnitude and (right) phase images were acquired orthogonal to nitinol stent in main pulmonary artery position. Presence of low-signal-intensity ring around pulmonary artery on magnitude image represents susceptibility artifacts derived from stent. High signal intensity within stent lumen on phase image is indicative of forward flow in pulmonary artery during systole.

all images and was useful for confirming the desired tip position of the guide wire in the pulmonary bed (Fig 2).

Functional and Morphologic Assessment of the Nitinol Stent

Nitinol stents were clearly visualized on MR images (Figs 3, 5). On balanced fast field-echo images, the signal-to-noise ratio was reduced within the stent lumen owing to the radio-frequency shielding effects of the stent. The signal-to-noise ratio in the center of the stent was significantly lower than that in the pulmonary artery distal to the stent (3.9 ± 0.5 vs 8.1 ± 1.9, respectively; $P < .01$). At the stent wall, a circumscribed signal void was a result of susceptibility artifacts (Figs 3, 5). The T1-weighted turbo field-echo sequence produced slightly less susceptibility artifacts (1.8 ± 0.6 pixels) than did the balanced fast field-echo sequence (2.4 ± 0.9 pixels, $n = 5$). Figure 6 shows a cross section of the nitinol stent as a low-signal-intensity ring on the magnitude image that surrounds brighter flowing blood on a phase image obtained during systole with velocity-encoding cine MR imaging.

In the animals with a stent placed distal to the pulmonary valve, pulmonary antegrade (4.9 ± 1.2 L/min/m^2), but no retrograde, blood flow was measured with velocity-encoding cine MR imaging. No pulmonary regurgitation was noted at angiography in these animals. MR imaging–guided peak systolic pressure measurements within the right ventricle (34 mm Hg ± 6) and pulmonary artery (22 mm Hg ± 6) were similar to those obtained with angiographic guidance (32 mm Hg ± 8 and 21 mm Hg ± 4, respectively).

In one animal, the retrograde pulmonary blood flow was measured within the stent lumen placed across the pulmonary valve. A pulmonary regurgitant fraction of 37% was determined from the ratio of pulmonary antegrade flow (5.1 L/min/m^2) to pulmonary retrograde flow (1.9 L/min/m^2). In the same animal, pulmonary angiography revealed severe pulmonary regurgitation. At autopsy, the positions and patency of the stents seen at MR imaging and angiography were confirmed in all cases. There was no evidence of any complication during stent placement (eg, stent damage, stent migration, vascular perforation, or intramural injury).

DISCUSSION

Major findings in the present feasibility study are as follows: (*a*) MR imaging has the potential to guide cardiopulmonary interventions, (*b*) stent delivery was achieved in all animals, and (*c*) no complication occurred during MR imaging guidance of the interventional procedure. In addition to the interventional aspects of MR imaging–guided stent deployment, the following information was obtained immediately after stent placement: (*a*) stent position and morphology and (*b*) quantitative pulmonary blood flow volumes within the stent lumen. Our preliminary results indicate that during one interventional MR imaging session, cardiovascular abnormalities (eg, pulmonary stenosis or insufficiency) can be assessed during and after treatment.

Infants and children with congenital heart diseases frequently undergo multiple cardiac catheterizations during their lives. This imposes enormous cumulative radiation exposure and causes a substantial risk for malignancies (18,19). This radiation exposure has been further increased by using fluoroscopy and angiography to guide and assess the results of transcatheter interventional procedures. MR imaging is now recognized as an attractive alternative to angiography for the pre- and postoperative assessment of many congenital heart defects. With the

introduction of improved magnetic gradient systems, fast imaging sequences have become possible. In the present study, we showed that interactive real-time MR imaging has the potential to guide stent placement in the pulmonary valve or main pulmonary artery and measure blood flow volume in the stent lumen immediately after the intervention.

The fast and reliable definition of catheters and guide wires is crucial for accurate MR imaging–guided cardiac interventions. Active catheter tracking methods and passive MR imaging guidance of metallic guide wires carry potential risks due to the heating effects of the radio-frequency conducting components (20–22). The nitinol guide wire used in this study was subject to potential heating during imaging. Heating effects might be produced with sequences with high flip angles and short repetition times (eg, the balanced fast field-echo sequence). In addition to safety issues related to heating, clear and complete imaging of catheters and guide wires is crucial to avoid looping or tip displacement, which may lead to vascular or cardiac injuries or procedure failure. In the present study, the shaft position of catheters and guide wires was achieved only for segments but not for their entire length, owing primarily to the tortuous course through the right ventricular outflow tract and pulmonary artery.

Several authors have reported the use of MR imaging–compatible catheters and guide wires (23,24). To our knowledge, however, none of the investigated instruments contained properties required for complex cardiovascular interventions, such as (*a*) fast and reliable detection of the tip; (*b*) curvature of the shaft; and (*c*) material properties such as tip flexibility, torque and tracking ability, shaft strength, and flexibility. More work is needed to develop new MR imaging–compatible catheters and guide wires that are appropriate for use in cardiovascular interventions. In the future, research methods such as use of resonance circuits as fiducial markers should be investigated to provide tip and shaft detection without incorporating the risk of heating effects inherent with active catheter tracking methods (25,26).

Occasionally, we were able to visualize the pulmonary valve with MR imaging. In these cases, the valves were used as a landmark for stent placement. The visualization of the leaflets in the present study may be attributed to the slow movement of the leaflets when interventional instruments are placed across the valve. It may be possible to continuously visualize the valve leaflets by using thinner sections. Visualization of the valves before the interventional procedure helps placement of the stents in the proper position.

In several studies, MR imaging has proved to be an accurate and reproducible method for assessing vascular hematoma and aneurysms (27). However, the assessment of complications due to stent placement in patients with vascular hematoma or aneurysms is problematic. Metallic stents cause (*a*) susceptibility artifacts, which are superimposed on the vascular wall; and (*b*) radio-frequency shielding effects, which reduce the MR signal inside the stent lumen. The degree of image distortion is related directly to the material and design properties of the stent (28). Use of a nitinol stent in our study caused only moderate susceptibility artifacts and radio-frequency shielding effects. Visualization of the entire vascular wall was not achieved. This pitfall may limit the ability to detect intramural injuries. The properties of the nitinol stent, however, did not vitiate the depiction of the stent or vascular morphology or the quantification of blood flow volumes within the stent lumen (16,17). In future research, it will be necessary to use MR imaging sequences and stent designs that further reduce MR signal void due to susceptibility and radio-frequency shielding.

In the diagnostic arena of congenital heart defects, MR imaging may supplement ultrasonography (US) in pre- and postoperative catheterization. The complementarily use of both techniques may reduce the need for pre- and postoperative catheterization. In general, US is cheaper than MR imaging, is widely available, and has excellent acoustic windows in infants. The one major limitation of US is that the hemodynamic parameters can be assessed only qualitatively.

In conclusion, the results of this preliminary study demonstrate that stent deployment in the pulmonary position is feasible with MR imaging guidance. Furthermore, postinterventional assessment of stent morphology and blood flow volumes within the stent lumen is possible with balanced fast field-echo and velocity-encoding cine MR imaging. Depending on the information required, MR imaging sequences and interventional instruments can be monitored sequentially to optimize images of background anatomy, frame rate, or contrast between interventional instrument and its surroundings.

Practical application: Radiation doses used in diagnostic and interventional pediatric cardiac catheterization are high. Stent deployment in the pulmonary system with MR imaging guidance can be applied in patients with obstructive right ventricular and pulmonary disease without the need for radiation. Furthermore, interventional MR imaging may be useful for assessing cardiopulmonary abnormalities, guiding cardiopulmonary interventions, and providing postinterventional evaluation.

References

1. Therrien J, Siu SC, McLaughlin PR, et al. Pulmonary valve replacement in adults late after repair of tetralogy of Fallot: are we operating too late? J Am Coll Cardiol 2000; 36:1670–1675.
2. Fogel AM, Rychik J. Right ventricular function in congenital heart disease: pressure and volume overload lesions. Prog Cardiovasc Dis 1998; 40:343–356.
3. Hosking MC, Benson LN, Nakanishi T, et al. Intravascular stent prosthesis for right ventricular outflow obstruction. J Am Coll Cardiol 1992; 20:373–380.
4. Bonhoeffer P, Boudjemline Y, Saliba Z, et al. Transcatheter implantation of a bovine valve in pulmonary position. Circulation 2000; 102:813–816.
5. Dolmatch BL, Blum U. Stent-grafts: current clinical practice. New York, NY: Thieme Verlag, 2000.
6. O'Laughlin MP, Slack MC, Grifka RG, et al. Implantation and intermediate-term follow-up of stents in congenital heart disease. Circulation 1993; 88:605–614.
7. Powell AJ, Lock JE, Keane JF, Perry SB. Prolongation of RV-PA conduit life span by percutaneous stent implantation: intermediate-term results. Circulation 1995; 92:3282–3288.
8. Pattynama PMT, de Roos A, van der Wall E, et al. Evaluation of cardiac function with magnetic resonance imaging. Am Heart J 1994; 128:595–607.
9. Caputo GR, Kondo C, Masui T, et al. Right and left lung perfusion: in vitro and in vivo validation with oblique-angle velocity-encoded cine MR imaging. Radiology 1991; 180:693–698.
10. Steffens JC, Bourne MW, Sakuma H, et al. Quantification of collateral blood flow in coarctation of the aorta by velocity encoded cine magnetic resonance imaging. Circulation 1994; 90:937–943.
11. Chung T. Assessment of cardiovascular anatomy in patients with congenital heart disease by magnetic resonance imaging. Pediatr Cardiol 2000; 21:18–26.
12. Manke C, Nitz WR, Djavidani B, et al. MR imaging–guided stent placement in iliac arterial stenosis: a feasibility study. Radiology 2001; 219:527–534.
13. Dion YM, El Kadi H, Boudoux C, et al. Endovascular procedures under near real-time magnetic resonance imaging guidance: an experimental feasibility study. J Vasc Surg 2000; 32:1006–1014.
14. Yang X, Bolster BD, Kraitchman DL, et al. Intravascular MR-monitored balloon angioplasty: an in-vivo feasibility study. J Vasc Interv Radiol 1999; 9:952–959.
15. Frahm C, Gehl HB, Lorch H, et al. MR

guided placement of a temporary vena cava filter: technique and feasibility. J Magn Reson Imaging 1998; 8:105–109.
16. Kuehne T, Saeed M, Reddy G, et al. Sequential MR monitoring of pulmonary flow with endovascular stents placed across the pulmonary valve in swine. Circulation 2001; 104:2363–2368.
17. Kuehne T, Saeed M, Moore P, et al. Influence of blood-pool contrast media on MR imaging and flow measurements in the presence of pulmonary arterial stents in swine. Radiology 2002; 223:439–445.
18. Modan B, Keinan L, Blumstein T, et al. Cancer following cardiac catheterization in childhood. Int J Epidemiol 2000; 29: 424–428.
19. Boothroyd A, McDonald E, Moores BM, et al. Radiation exposure to children during cardiac catheterization. Br J Radiol 1997; 70:180–185.
20. Ladd ME, Quick HH, Debatin JF. Interventional and intravascular imaging. J Magn Reson Imaging 2000; 12:534–546.
21. Konings MK, Batrtels LW, Smits HFM, et al. Heating around intravascular guidewires by resonating RF waves. J Magn Reson Imaging 2000; 12:79–85.
22. Liu CY, Farahani K, Lu DSK, et al. Safety of MRI-guided endovascular guide wire applications. J Magn Reson Imaging 2000; 12:75–78.
23. Backer CJ, Smits HF, Bos C, et al. MR-guided balloon angioplasty: in vitro demonstration of the potential of MRI for guiding, monitoring, and evaluating endovascular intervention. J Magn Reson Imaging 1998; 8:245–250.
24. Yang X, Atalar E. Intravascular MR imaging–guided balloon angioplasty with an MR imaging guide wire: feasibility study in rabbits. Radiology 2000; 217: 501–506.
25. Wong EY, Zahng Q, Duerk JL, et al. An optical system for wireless detuning of parallel resonant circuits. J Magn Reson Imaging 2000; 12:632–638.
26. Kuehne T, Fahrig R, Scott G, et al. Passive position monitoring of endovascular catheters with integrated resonant circuit under interactive real-time MRI guidance (abstr). Radiology 2001; 221(P):429.
27. Higgins CB, Hricak H, Helms CA. Magnetic resonance imaging of the body. Philadelphia, Pa: Lippincott-Raven, 1996; 519–553.
28. Lehnhart M, Voelk M, Nitz WR, et al. Stent appearance at contrast-enhanced MR angiography: in vitro examination with 14 stents. Radiology 2000; 217:173–178.